5. THE EARLY IRON AGE ELITE BURIAL FROM FRANKFURT AM MAIN, STADTWALD: A NEW CRANIAL RECONSTRUCTION AND PALEOPATHOLOGICAL REANALYSIS

Carolin Röding[1]*, Liane Giemsch[2]

[1]*Paleoanthropology, Senckenberg Centre for Human Evolution and Palaeoenvironment, Eberhard Karls University of Tübingen, Rümelinstraße 23, Tübingen 72070, Germany*
[2]*Archäologisches Museum Frankfurt, Karmelitergasse 1, Frankfurt am Main 60311, Germany*
**carolin.roeding@uni-tuebingen.de*

https://dx.doi.org/10.15496/publikation-66861

KEYWORDS | Early Iron Age, virtual reconstruction, paleopathology, differential diagnosis, asymmetry

ABSTRACT

The Early Iron Age chieftain from Frankfurt am Main, Germany, is one of the most important Iron Age gravefinds in Central Europe. It was excavated in 1966/67 and represents a remarkable discovery. An almost complete skeleton together with grave goods, was found in an undisturbed burial mound. The archaeological material is dated to around 700 BCE and therefore one of the oldest known burials of the Early Iron Age elite. The skeletal remains are fragile but allowed for an age estimation of around 50 years at death, while the sex was estimated as male.

Here, we present a new reconstruction of the fragmented cranium of the chieftain based on virtual anthropological methods. Furthermore, a study of bilateral asymmetry was carried out on the reconstructed cranium, the 2nd cervical vertebra, and the humeri, in order to explore the possible impact of a healed trauma in the left clavicle on the other skeletal elements. Bilateral cranial linear measurements and surface distance maps between bones and their bilateral counterparts suggest only slight to moderate restrictions in the range of motion caused by the healed trauma.

The 3D print of the presented virtual cranial reconstruction together with a facial reconstruction and the original skeletal remains will be on display in a museum context, together with the archaeological material, which will make the Early Iron Age chieftain more accessible to the museum visitors.

5.1 INTRODUCTION

One of Frankfurt's most important prehistoric finds is the Early Iron Age chieftain burial from mound

Michael Francken, Katerina Harvati (Hrsg.), Facetten der Osteologie. Festschrift zu Ehren von Prof. Dr. Joachim Wahl. Tübingen University Press, Tübingen 2023. https://dx.doi.org/10.15496/publikation-66865

I of the Eichlehen burial mound group in the eastern urban forest (Stadtwald), located at today's city border with Offenbach. The burial mound, associated with a stone stele, was located in the middle of more than 50 grave mounds (Fischer, 1979). The grave was excavated in 1966/67 from the originally 3.5 meter high burial mound with a diameter of 36 meter. The excavation was led by Ulrich Fischer, the director of the Museum of Pre- and Protohistory, which is today's Archäologisches Museum Frankfurt (Hofmann, 2010). It quickly became clear that the richly appointed central grave had to be a burial of a socially outstanding male individual. Among other gifts, the grave included a bronze sword, a chape of a scabbard, a precious wooden double yoke with leather cover and bronze fittings with bridle and harness for a horse team, a luxurious banquet and drinking set made of bronze, an exquisite iron butcher knife with a gold insert, and a situla made of sheet bronze.

Based on typological considerations of the grave goods, in particular the bronze sword of type »Mindelheim«, the shape of the sheath chape, and the »Schälchenkopf«-needles, the chieftain burial dates to the Early Iron Age stage Hallstatt CIb, which indicates a date around 700 BCE (Willms, 2002; Fischer, 1979).

The burial complex is one of the oldest known burials of the Early Iron Age elite, about 170 years older than the grave of the »Chieftain of Hochdorf« (Krausse, 1996) and 250 years older than the grave of the »Chieftain of Glauberg« (Herrmann and Frey, 1996; Baitinger, 2010).

Most grave goods were found near the walls of the burial chamber with some distance to the skeletal remains. The skeletal remains lie in a supine position, relatively central in the burial chamber. The bronze sword was found at the right side of the skeleton, in close proximity to the remains (for illustration see Fischer, 1979: Plan 7).

The skeletal remains are fragile but allowed for a comprehensive osteological reanalysis in their today's repository at the Archäologisches Museum Frankfurt (Willms, 2002; Rehbach et al., 2003). Following criteria established by Ferembach et al. (1979) the sex was estimated as male and the age of the individual was estimated to be around 50 years at death. A stature of circa 175 cm was calculated following methods established by Pearson (1899). Several degenerative changes associated with an advanced age were reported, especially in the preserved *lumbar vertebrae*, the left *acetabulum*, and the corresponding left *caput femoris*. The left *corpus claviculae* shows a healed trauma between the *tuberculum conoideum* and the *tuberositas ligamentum costoclavicularis*. The two parts of the clavicle did not heal in an *anatomically* correct position. A roughly 30 degree angle can be observed between the *pars acromialis* and the *pars sternalis* of the clavicle. Consequently, restrictions of the range of motion in the left arm are expected. In addition, Rehbach et al. (2002) reported that the right *corpus humeri* had a diameter 2 mm greater than the left *corpus humeri*. The cranium was excluded from the reanalysis due to severe taphonomic deformations and fragmentation, probably caused by the collapse of the burial chamber (Rehbach et al., 2002).

In this chapter, we aim to complete the overall picture of the osteological analysis from 2002. The first goal is to present a virtual cranial reconstruction of the Early Iron Age chieftain, thereby enabling the inclusion of the cranium in the osteological analysis. Furthermore, in order to further explore the possible impact of the healed trauma in the left clavicle, analyses of asymmetry on the bones surrounding the left clavicle were carried out.

5.2 VIRTUAL CRANIAL RECONSTRUCTION

The cranium was manually reconstructed in the past and is represented as two parts, (1) the neurocranium and right *os zygomaticum*, and (2) the *mandibula*, *maxillae* and *ossa nasalia* (Figure 1). Fragments are attached to each other and the tooth rows of maxilla and mandible are fixed in occlusion by glue. The glue is non-soluble by water. In order to minimize damage to the cranial fragments, the new reconstruction presented in this manuscript

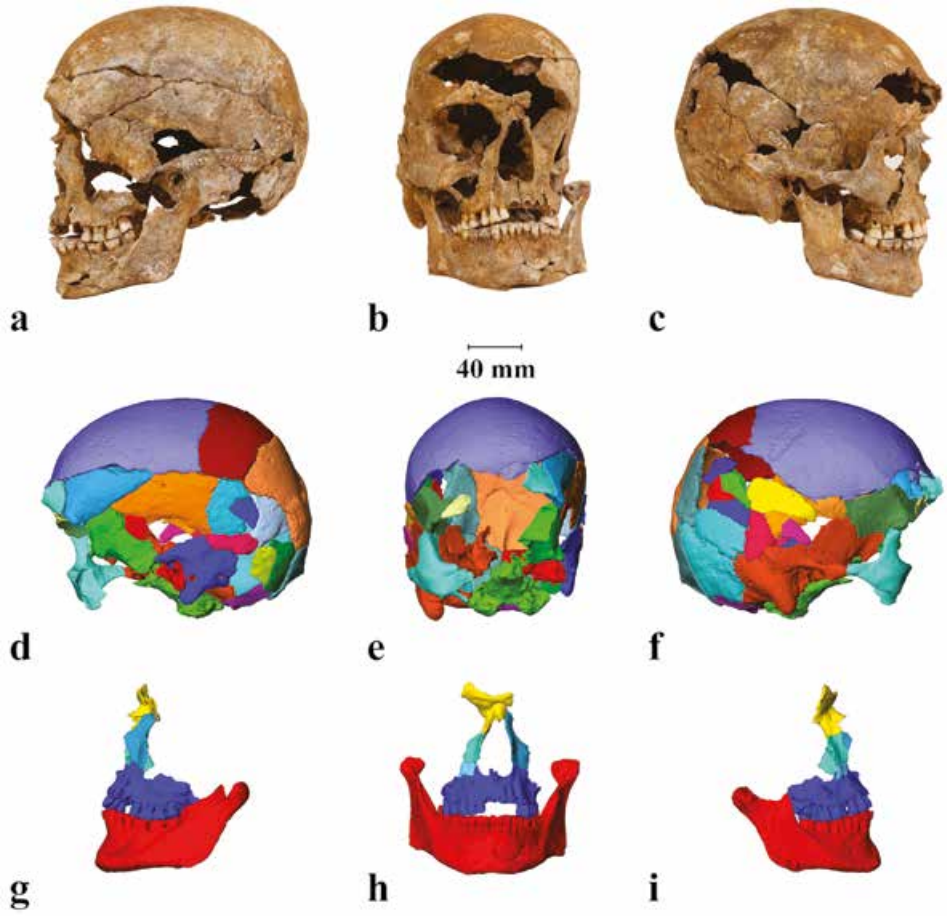

Figure 1: (a-c) photographs of the original osteological remains by U. Dettmar on behalf of the Archäologisches Museum Frankfurt; illustrations of segmented fragments of the (d-f) neurocranial and (g-i) facial scan in original position; each shown in anterior view (b,e,h), lateral view from the right (c,f,i) and from the left (a,d,g).

was carried out in a virtual environment, based on data obtained with computed tomography (CT). The two parts of the cranium were scanned at the Paleoanthropology Department of the University of Tübingen, using an industrial »General Electric Phoenix« µCT scanner (model v|tome|x). The CT scans of both parts show isotropic voxel sizes of 0.28535 mm. All segmentation and reconstruction steps as well as linear measurements described below were carried out in Avizo (FEI Visualization Sciences Group) and the Resample software from the New York Consortium in Evolutionary Primatology (NYCEP, http://pages.nycep.org/nmg/programs.html).

Prior to the reconstruction, each fragment was segmented separately to allow independent movement. Differences in material density between bone fragments and glue in the CT scans were insufficient for threshold based automated segmentation. Thus, each fragment was segmented manually slice by slice to ensure accurate separation between materials. In total, 40 fragments were segmented (Figure 1d-i).

In the first step of virtual reconstruction, two different reconstruction protocols were used, bilateral symmetry and smooth curvature (for comparison, see Zollikofer et al., 2005; Figures 2 and 3a,d). Cracks between fragments were not closed completely in this step unless the breakage patterns matched perfectly, in order to account for possible alterations of the edges of the fragments. No reference cranium was used due to preserved anatomical features covering almost the entire cranial anatomy.

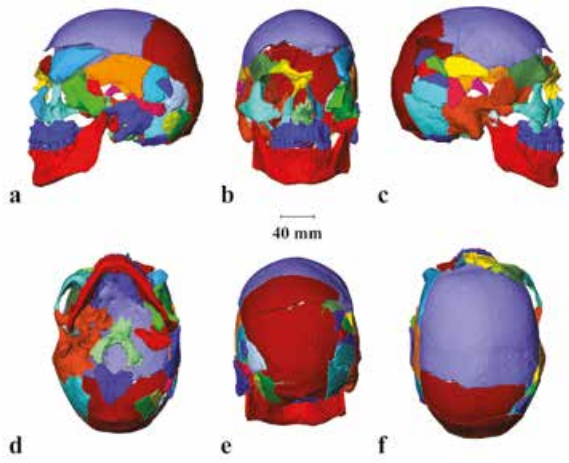

Figure 2: illustration of the first step of virtual reconstruction; shown from (a) lateral left, (b) anterior, (c) lateral right, (d) inferior, (e) posterior and (f) superior view.

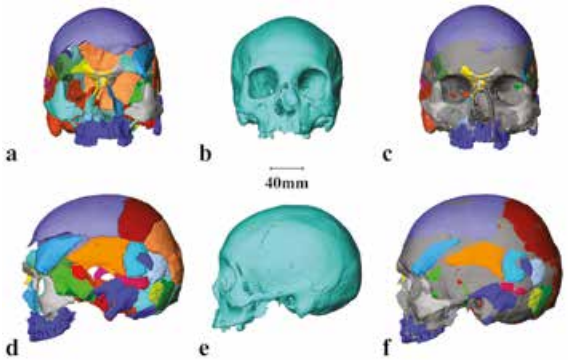

Figure 3: illustration of (a and d) the first step of virtual reconstruction with mirrored fragments shown as grey areas, (b and e) modern human reference cranium used in warping, and (c and f) reconstruction after warping; shown in anterior view (a-c) and lateral view from the left (d-f).

Shared features of chordates are approximate bilateral cranial symmetry and smooth curvature on the ectocranial surface, especially in the neurocranium. When the position of fragments had to be corrected in order to deal with taphonomic distortion, smoothness was prioritized over bilateral symmetry. The anterior right part of the neurocranium was chosen as a starting point, as it presented a low amount of taphonomic deformation. All reconstructed fragments of the right side were duplicated and mirrored along the midsagittal plane onto the left side. This mirrored duplicate was used as a reference for the reconstruction of the fragments from the distorted left side of the neurocranium. The bicondylar width of the mandible was used as a control for cranial breadth at the mandibular fossae of the temporal bones. In reconstructing facial symmetry, the midsagittal plane of the neurocranium was used as a reference. The preserved fragments, located primarily on the left facial side, were reconstructed following the assumption of smooth curvature between fragments. Missing areas, such as the right *os zygomaticum*, the left *processus condylaris* of the mandible, and the right medial part of the *margo supraorbitalis ossis frontalis* were reconstructed by duplicating and mirroring their preserved bilateral counterpart (Figures 3a,d and 4).

After the first step the virtual reconstruction retains gaps between preserved fragments. For standard osteological analyses this reconstruction was sufficient. However, as the virtual reconstruction will be used in a museum context, further reconstruction was deemed necessary in order to enable 3D printing and ultimately to make the final reconstruction more accessible to museum visitors. The method of choice for further reconstruction was the geometric warping (Bookstein, 1989) of a reference cranium onto the manual reconstruction of the Iron Age chieftain (Figure 3). This method allows for subsequent 3D printing with a minimum of additional working steps.

The choice of the reference is crucial for the geometric warping. While size differences between reference and target, do not influence the outcome, shape differences do influence the warping of areas not represented in the target. To optimally match the shape of the reconstruction, a total of 37 CT scans from adult modern humans from central Europe housed in the osteological collection of the University of Tübingen were analyzed. Three metric indices based on linear measurements defined by Martin (1928) were evaluated, the ratio of cranial width (M8a) to length (M1d), ratio of orbit height (M52) to width (M51) as well as the ratio between upper facial height (M48) and width (M45). Overall cranial morphology was sufficiently matched by three reference crania. The chosen reference CT scans do not include the mandible.

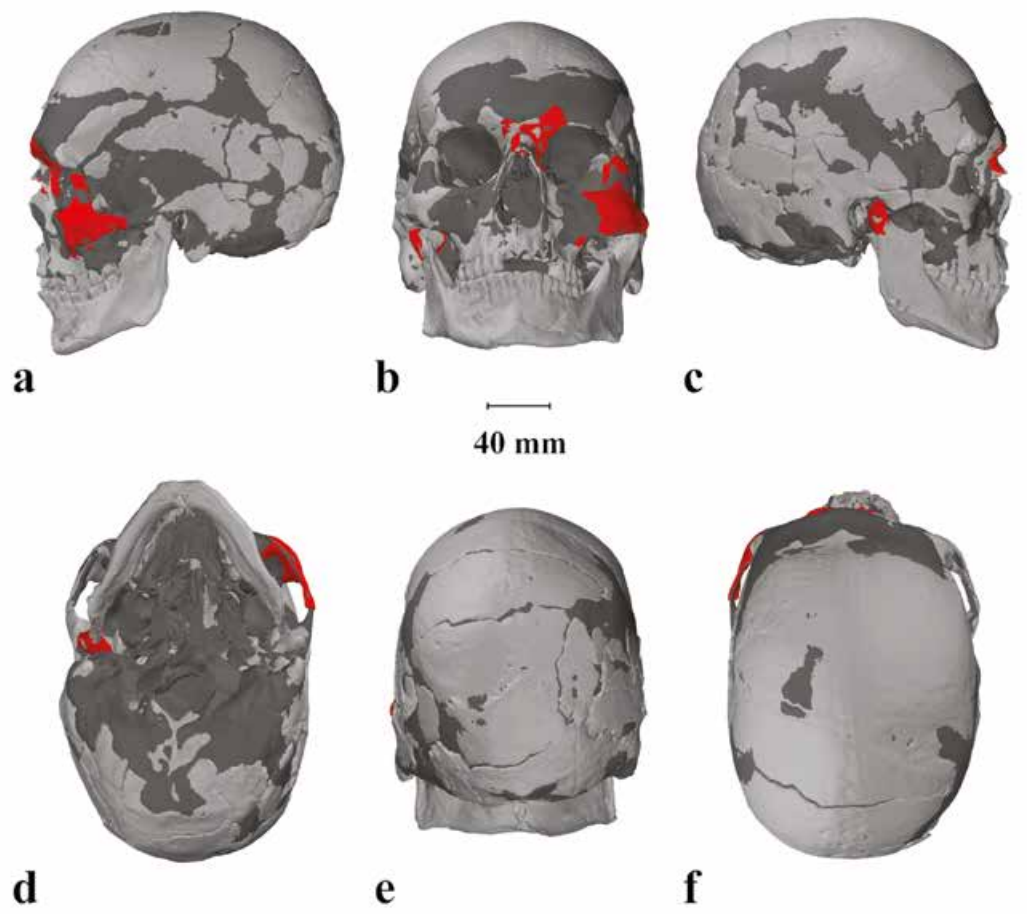

Figure 4: illustrations of the final virtual cranial reconstruction; shown from (a) lateral left, (b) anterior, (c) lateral right, (d) inferior, (e) posterior and (f) superior view; fragments shown in light grey are preserved in the original osteological material, in dark grey areas completed by warping and in red fragments mirrored during the first step of virtual reconstruction.

Therefore, the mandible was excluded from the reconstruction during the geometric warping. A 3-dimensional set of 39 homologous fixed anatomical points, often called landmarks, as well as 62 equidistant points on curves, such as the lambdoid or coronal sutures, were digitized on the target cranium and all three reference crania (for discussion see e.g. Zelditch, 2012; Slice, 2007; Bookstein, 1997; Mitteroecker and Gunz, 2009; Gunz and Mitteroecker, 2013). Differences in the position of homologous landmarks between the target and one reference at a time are calculated and captured in form of a matrix. Following the same matrix, the surface of the reference is deformed to match the target. In areas without landmark information due to missing fragments in the reconstruction, the deformation of the reference is interpolated based on Bookstein principle warps (Bookstein, 1989). The three reconstructions differed most in areas that were lacking landmarks or covered by a low number. The lack of landmarks at the s*quama frontalis* and the *ossa parietalia* led to mismatches between the warped reference and preserved fragments of the target. The reconstruction that had a minimal number of mismatches, was selected for 3D printing (Figures 3c,f and 4). For the final reconstruction, the mandible was added (Figure 4).

5.3 CRANIAL ASYMMETRY

All steps of the virtual reconstruction retain some distortion in the basicranium that could not be resolved with the reconstruction criteria (Figures 2d

and 4d). In addition, the *processus mastoidei* appear rather asymmetric during visual inspection. To test whether the bilateral difference in size between the *processus mastoidei* might be the result of normal cranial bilateral asymmetry, the two largest originally preserved fragments of the *os temporale* were analyzed.

The largest fragment of the right *os temporale* preserves the *pars tympanica*, a part of the *squama temporalis*, the *pars mastoidea* including the *processus mastoideus* as well as the majority of the *pars petrosa*. In contrast, the largest fragment of the left *os temporale* preserves only the *pars tympanica* and the lateral bony table of the *pars mastoidea* including the *processus mastoideus*. The *squama temporalis* is almost completely missing on the left side and the *pars petrosa* is represented by a separate smaller fragment. The two largest temporal fragments have a great effect on basicranial shape, especially due to a lack of preserved structures in the left posterior basicranium.

To explore bilateral asymmetry, data was collected in form of linear measurements (Table 1) and as distance map between the surfaces of the two largest temporal fragments (Figure 5). The distance map was calculated as the difference in millimeter per surface triangle of virtual surface meshes created from the CT scans (see section about segmentation). The differences are translated as colors for illustration (Figure 5). Greatest differences between the fragments were found along the crest on the *processus mastoideus* and *supramastoid crest*. In contrast, the absolute length of the mastoid process differs less than one millimeter.

Following measurement definitions from Helmuth (1968) three bilateral linear measurements were digitized on both the CT scans of the chieftain and a comparative sample of 32 CT scans from adult modern humans from central Europe housed in the osteological collection of the University of Tübingen. For all measurements, the cranium was oriented in left or right lateral view, depending on the measurement in question, and in the Frankfurter Horizontal plane. The sagittal length was measured in millimeter parallel to the

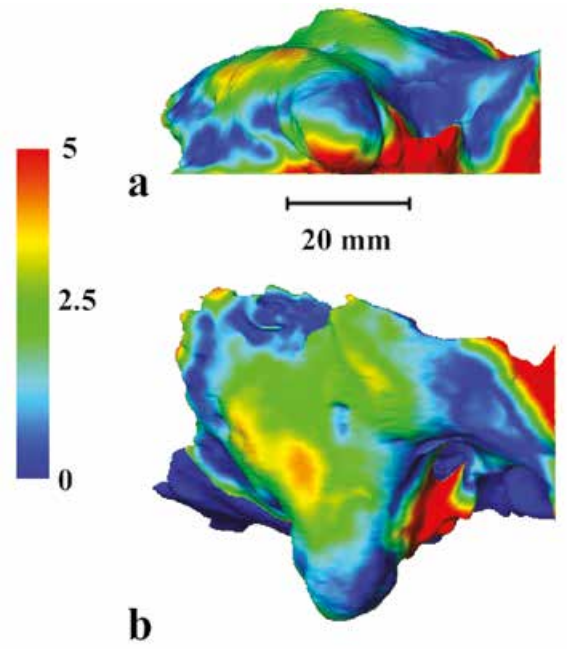

Figure 5: distance map ossa temporalia; shown from (a) inferior and (b) lateral right view; distances in mm translated to color code ranging from no difference in blue to ≥ 5 mm difference in red.

eye-ear-plane (EEP) starting at the inferior margin of the *meatus acusticus externus* to the posterior end of the *processus mastoideus*. The height of the processus was measured in millimeter from the most inferior point to porion (for landmark definition see Martin, 1928). The third measurement captures the angle between the *processus mastoideus* and the EEP in degree. The angular arm on the mastoid process is constructed by dividing the processus into two equal parts outgoing from the most inferior point.

Statistics were calculated in R (R Development Core Team, 2014) and include means and standard deviations for each measurement grouped by sex as well as asymmetry calculated as the absolute difference between corresponding bilateral measurements (Table 1). Single measurements can vary substantially between individuals, between sexes and within one sex, whereas the majority of individuals show bilateral asymmetries of less than three millimeter respectively degrees. Overall, two of the three measurements in the chieftain are more asymmetric than the mean. However, the maximal

Measurement	Sagittal Length	Sagittal Length	Height	Height	Angle Process to OAE	Angle Process to EEP	Difference Sagittal Length	Difference Height	Difference Angle Process to EEP
Measured Side	R	L	R	L	R	L	R-L	R-L	R-L
Female	21.291	19.904	28.932	28.055	56.87	57.86	1.527	1.727	2.37
	± 4.318	± 4.314	± 2.394	± 2.207	± 7.770	± 6.284	± 1.719	± 1.131	± 2.679
Male	20.175	19.344	29.666	28.867	55.9	56.034	1.678	1.088	2.2
	± 4.553	± 4.035	± 3.245	± 3.243	± 5.267	± 5.043	± 1.689	± 1.135	± 1.946
Maximum of Whole Sample	30.72	28.1	35.01	35.22	75.2	70.7	7.85	4.32	9.1
Early Iron Age Chieftain	16.55	16.17	36.51	33.38	54.2	47.3	0.38	3.13	6.9

Table 1: bilateral cranial linear measurements; shown as mean and standard deviation per sex as well as the maximum per measurement; all measurements in mm or degree.

bilateral differences measured in this specific comparative sample exceeded the measurements from the chieftain.

5.4 POSTCRANIAL ASYMMETRY

As described in the osteological reanalysis from 2002 (Rehbach et al., 2002) the left clavicle shows a roughly 30 degree angle between the *pars acromialis* and the *pars sternalis* (Figure 6). The trauma occurred pre-mortem, as indicated by the formation of callus as physiological reaction to the trauma. The surface structure of the bone as well as the radiographic image in Willms (2010) suggest at least 12 weeks of healing, but it is quite likely that years passed between the breakage of the clavicle and time of death (Gerstenfeld et al., 2003; Einhorn, 1998).

Several large muscles important for the head and arm movement originate or insert on the clavicula, including the *musculus trapezius*, *musculus deltoideus*, *musculus sternocleidomastoideus* and *musculus pectoralis major*. Each of these muscles could possibly be affected directly by trauma in the clavicle or indirect due to complications in the

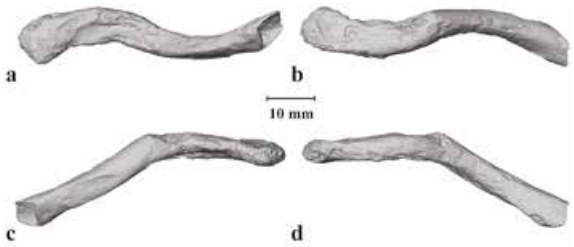

Figure 6: surface model of left clavicle from a surface scan made by an Artec Space Spider handheld 3D scanner; shown in (a) inferior, (b) superior, (c) anterior and (d) posterior view.

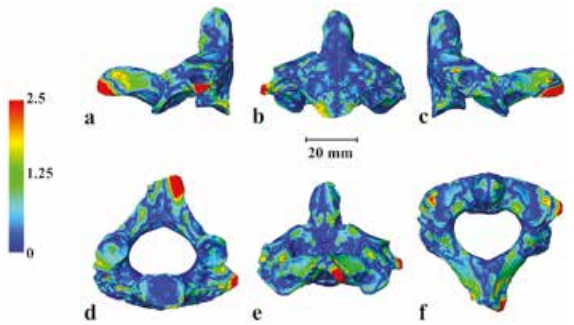

Figure 7: distance map axis, 2nd cervical vertebra; shown from (a) anterior, (b) inferior, (c) lateral left, (d) posterior, (e) superior and (f) lateral right view; distances in mm translated to color code ranging from no difference in blue to ≥ 2.5 mm difference in red.

healing process of a trauma. Under the assumption that the time of death took place several years after the trauma, other skeletal elements would show bone resorption at muscle attachments due to permanently damaged muscles. Not all skeletal elements involved in the attachment of the muscles listed above are preserved in the chieftain. The bones that are preserved are the humeri and the 2nd cervical vertebra (axis). These elements were surface scanned with an Artec Space Spider handheld 3D scanner.

None of the previously discussed muscles directly attaches to the axis. However, the lateral surface of the mastoid process represents the insertion site of the *musculus sternocleidomastoideus*. In case the observed bilateral asymmetry in this particular area was caused by differences in physical stress initiated by this muscle, a very strong bilateral imbalance would have led to a difference in degeneration between right and left in the cervical vertebrae. As shown in Figure 7, the only preserved cervical vertebra shows no bilateral asymmetry. Here, the distance map was calculated between the original surface scan of the axis and its mirrored duplicate in order to compare the right and left halves. In contrast, the distance map calculated between the surface scans of the humeri shows bilateral asymmetry (Figure 8). The asymmetric areas are clearly limited to regions of muscle attachments. With a maximum of around 5.5 mm, the greatest asymmetry was found at the lateral upper third of the humerus at the *tuberositas deltoidea*, where the *musculus deltoidea* inserts. The second area of asymmetry was found on the lower two thirds of the medial side extending to the anterior lower half of the humerus, respectively representing the origin of the *musculus brachialis* and insertion of the *musculus coracobrachialis*.

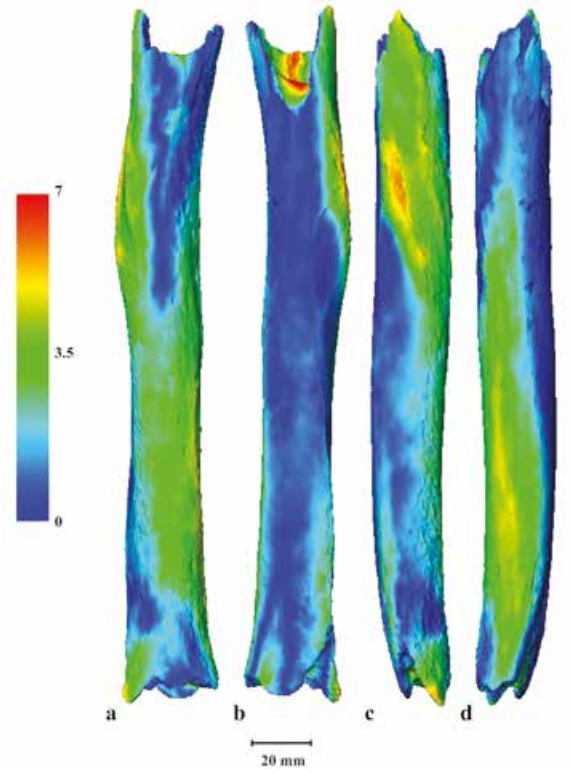

Figure 8: distance map humeri, shown from (a) anterior, (b) posterior, (c) lateral and (d) medial view; distances in mm translated to color code ranging from no difference in blue to ≥ 7 mm difference in red.

5.5 DISCUSSION

In response to their environment bones grow and remodel throughout life. This relationship was first described by Julius Wolff and is today known as Wolff's law (Wolff, 1893). Following Wolff's law, increased mechanical stress should lead to bone growth and remodeling. However, the relationship between skeletal stress markers, like muscle attachments, and an adult activity pattern is not always straight forward due to multicausality in the formation of stress markers (for discussion see Ruff et al., 2006; Pearson and Liebermann, 2004). In an archaeological context, taphonomy can further complicate the interpretation of osteological remains due to chemical as well as mechanical postmortem alteration of the bones.

Three possible causes for the basicranial distortion in the virtual reconstructions and the seemingly asymmetric mastoid processes are discussed here. Due to the very fragmented nature of the cranial remains, taphonomy is the first point to take into consideration as the probable cause. Overall, the cranial fragments are fragile but well preserved. With the exception of the fragments

comprising the left *os temporale*, all fragments preserve intact ectocranial surfaces. Due to taphonomy on the medial portion of the left *processus mastoideus*, indicated by exposed spongiosa, this structure appears more gracile in its medio-lateral diameter than its bilateral counterpart. Taphonomic deformation of other temporal fragments was not observed. In addition, the reconstruction of the anterior vault, based on smooth continuation between fragments, matched the preserved bicondylar width of the mandible, which suggest that deformation of the fragments of the anterior vault is highly unlikely. Slight deformation in the fragments of the posterior cranial vault cannot be completely ruled out due to large missing areas lateral and posterior to the *foramen magnum*. Missing fragments could be the cause for basicranial distortion due to missing reference points in the reconstruction of the position of preserved fragments, such as the *pars basilaris ossis occipitalis* (Figure 2d).

The combination of cranial deformation and asymmetries in the mastoid processes described in this manuscript could be part of the osteological manifestation of torticollis. Torticollis is a collective term for diseases caused by an asymmetrically-shortened *musculus sternocleidomastoideus* and can either be congenital or acquired during life (Tomczak and Rosman, 2012). The shortened muscle leads to a twisting of the head and neck as well as tilting the head towards the direction of the affected muscle and rotating the chin in the opposite direction. Rotation of the chin often results in asymmetric tooth abrasion (Pirttiniemi et al., 1989; Chung-Chih et al., 2004) and twisting of the neck over an extended time period would lead to asymmetries in the cervical vertebrae (Chawda et al., 2000). In additon to the secondary osteological manifestations, congenital torticollis is often accompanied by cranial and facial asymmetries. In archaeological contexts, congenital torticollis with cranial deformation, represented by a plagiocephalus has been proposed for several Celtic individuals (Müller et al., 2008) and the hominin cranium from Salé (Hublin, 2002). Plagiocephaly describes a cranial deformation that involves a unilateral, flattened back of the head. In severe cases, this is accompanied by an anterior shift of the ipsilateral ear region and ipsilateral frontal bulging (Gautschi et al., 2013). In case of the chieftain, no plagiocephalus and no asymmetry in the preserved cervical vertebra (Figure 7) were found and neither the mandible nor the maxilla show asymmetric tooth abrasion.

Although the insertion of the *musculus sternocleidomastoideus* at the lateral side of the mastoid process shows asymmetry (Figure 5), the maximal bilateral differences measured in the reference sample exceeded the measurements from the Iron Age chieftain and classify the asymmetry as pronounced but not unusual.

All in all, the most plausible cause for the basicranial deformation and asymmetry of the cranium, especially in the area of the mastoid processes, is a combination of taphonomy, slight deformation as well as missing fragments, and normal bilateral asymmetry.

Asymmetry in muscles and their mass, so called muscle imbalance, can occur at all intensities, ranging from light forms not detectable on osteological remains to severe forms like the above discussed torticollis. An imbalance in bilateral muscle mass can have several causes including one-sided muscle atrophy or hypertrophy due to differences in use between both sides (Boonyarom and Inui, 2006). One head of the *musculus sterneocleidomastoideus* originates at the superior border and anterior surface of the medial third of the clavicle and inserts at the *processus mastoideus.* This connects the less robust muscle attachment at the left *processus mastoideus* with the trauma in the left clavicle. However, no bilateral differences were found at the muscle attachments on the medial part of both left and right clavicles.

The lateral third of the clavicle forms the insertion site for one head of the *musculus trapezius*. Due to the trauma in the left clavicle, direct comparison of the muscle attachments at the insertion was not possible. The origin of the *musculus trapezius* at the *linea nuchalis superior*, *protuberantia oc-*

cipitalis externa and *crista occipitlais externa* is distributed on multiple preserved cranial fragments (Figure 2d,e). The manifestation of the lateral superior nuchal lines is weak while the *protuberantia occipitalis externa* and the *crista occipitalis externa* show a pronounced manifestation and are slightly skewed to the right. This combination suggests a muscle imbalance with a slightly stronger right trapezius muscle. In general, the healed trauma in the clavicle seemed to have no significant impact on the muscles involved in the movement of the head, and all differences between the left and right sides can be attributed to normal variation

Pronounced differences were found at the preserved humeral diaphyses (Figure 8). The insertion of the *musculus deltoidea*, the origin of the *musculus brachialis*, as well as the insertion of the *musculus coracobrachialis* exhibit the greatest bilateral differences from around 2 to 5.5 mm. The *musculus pectoralis major*, which originates at the medial half of the clavicle, could not be completely analyzed as only the most distal part of its insertion is preserved on the humeral fragments. The preserved area shows an asymmetry of around 3.5 to 4 mm whereas large parts of the humeri differ by less than one mm. The overall similar dimensions of the humeri suggest normal ontogenetic development as congenital pathologies effecting muscle development would secondarily affect overall bone robusticity during ontogeny (e.g. Rodríguez et al., 1988).

In the case of the chieftain, two causes or their combination are plausible in explaining bilateral asymmetries acquired during adulthood. First, muscle atrophy caused by the restricted use of the left arm. The osteological analyses showed that the healed trauma at the left clavicle is expected to limit the range of motion in the left arm (Rehbach et al., 2002). Disuse of muscles leads to muscle atrophy (Boonyarom and Inui, 2006) and, following Wolff's law, remodeling and ultimately reduction of the muscle attachment area according to the reduced mechanical stress. Second, muscle hypertrophy at the right arm induced by carrying a sword. It has been proposed that the Iron Age chieftain used the right arm in order to carry and use his sword (Rehbach et al., 2002). This suggestion is supported mainly by the archaeological context. The bronze sword was found in close proximity to the right-sided osteological remains. Use of a sword could lead to a muscle hypertrophy and consequently growth and remodeling of the muscle attachment area. The affected muscle attachments belong to muscles that are involved in adduction and flexion of the arm as well as its inward rotation, and flexion of the forearm at the elbow (Schünke, 2000). While patterns of skeletal stress markers cannot be directly correlated with a single activity pattern, the listed movements do not contradict the proposed hypertrophy. Overall, the archaeological remains support the second hypothesis while the preserved osteological remains do not allow to favor one hypothesis, thereby making a combination of both hypotheses the most plausible explanation for the here observed bilateral asymmetries in the humeri.

5.6 CONCLUSION

The new virtual cranial reconstruction of the Early Iron Age chieftain from Frankfurt am Main presented in this manuscript allowed the analysis of several cranial features as well as muscle attachments, linking cranium and post-cranium. Thereby the analysis of the possible impact of the dislocated clavicle onto surrounding skeletal elements could be extended compared to a former study (Rehbach et al., 2002). The dislocated clavicle was found to have no significant impact on the muscles involved in head movement as bilateral differences in the cranium can be attributed to either normal variation or taphonomy. In case of the humeri, a combination between muscle atrophy in the left arm caused by the trauma in the clavicle and muscle hypertrophy in the right arm induced by carrying a sword is the most plausible explanation for the observed bilateral asymmetries.

As the burial complex is one of the oldest known burials of the Early Iron Age elite it plays an important role in better understanding the so-

cial structure as well as health status of that time period. The chieftain was of rather large as well as robust stature and reached by standards of the time a grate age (Rehbach, 2003). Osteological evidence suggests an overall good health status and most probably only slight to moderate limitations in range of motion of the left arm. The combination of the new and previous results based on the study of osteological and archeological remains provides a valuable snapshot in time of a socially outstanding male individual.

Within the context of the museum, the Early Iron Age chieftain can help to make this particular archaeological time period more accessible to the public. The reconstruction presented here will allow for the production of a 3D print and a facial reconstruction, and will be featured in the Archäologisches Museum Frankfurt, together with the osteological remains and the archaeological material.

ACKNOWLEDGEMENTS

Many thanks to H. Scherf and K. Harvati for making this collaboration possible. We would like to thank M. Francken in his role as curator of the anatomical collection of the University of Tübingen for providing access to reference samples. In addition, we would like to acknowledge the assistance of the Paleoanthropology High Resolution Computing Tomography Laboratory at the Eberhard-Karls-Universität Tübingen, supported in part by the DFG INST 37/706-1, in scanning the Early Iron Age chieftain as well as the reference sample.

REFERENCES

Baitinger, H., Kresten, P., 2010. Der Glauberg ein Fürstensitz der Späthallstatt-/Frühlatènezeit in Hessen. Glauberg Studien, Vol. 1. Selbstverleger des Landesamtes für Denkmalpflege Hessen, Wiesbaden.

Bookstein, F.L., 1989. Principal Warps: Thin-Plate Splines and the Decomposition of Deformations. IEEE Transactions on Pattern Analysis and Machine Intelligence 11, 567-85.

Bookstein, F.L., 1997. Morphometric Tools for Landmark Data: Geometry and Biology. Cambridge University Press, Cambridge.

Boonyarom, O., Inui, K., 2006. Atrophy and Hypertrophy of Skeletal Muscles: Structural and Functional Aspects. Acta Physiologica 188, 77-89.

Chawda, S.J., Münchau, A., Johnson, D., Bhatia, K., Quinn, N. P., Stevens, J., Lees, A. J., Palmer, J. D., 2000. Pattern of Premature Degenerative Changes of the Cervical Spine in Patients with Spasmodic Torticollis and the Impact on the Outcome of Selective Peripheral Denervation. Journal of Neurology, Neurosurgery and Psychiatry 68, 465-71.

Einhorn, T.A., 1998. The Cell and Molecular Biology of Fracture Healing. Clinical Orthopaedics and Related Research 355, S7-S21.

Ferembach, D., Schwidetzky, I., Stloukal, M., 1979. Empfehlungen für die Alters- und Geschlechtsdiagnose am Skelett.(Recommandations pour le Diagnostic de l'âge et du Sexe sur les Squelettes). Homo Gottingen 30, 1-32.

Fischer, U., 1979. Ein Grabhügel der Bronze- und Eisenzeit im Frankfurter Stadtwald. Schriften des Frankfurter Museums für Vor- und Frühgeschichte, Vol. 4. W. Kramer, Frankfurt am Main.

Frey, O.H., Herrmann, F. R., Bartel, A., Kreuz, A., Rösch, M., 1997. Ein Frühkeltischer Fürstengrabhügel am Glauberg im Wetteraukreis, Hessen: Bericht über die Forschungen 1994-1996. Germania: Anzeiger der Römisch-Germanischen Kommission des Deutschen Archäologischen Instituts 75, 459-550.

Gautschi, O.P., Rilliet, B., Schaller, K., Jenny, B., 2013. Lagebedingter Plagiocephalus im Säuglingsalter: Diagnose und Behandlung. PRAXIS 102, 1537-42.

Gerstenfeld, L.C., Cullinane, D.M., Barnes, G.L., Graves, D.T., Einhorn, T.A., 2003.

Fracture Healing as a Post Natal Developmental Process: Molecular, Spatial, and Temporal Aspects of Its Regulation. Journal of Cellular Biochemistry 88, 873-84.

Gunz, P., Mitteroecker, P., 2013. Semilandmarks: A Method for Quantifying Curves and Surfaces. Hystrix, the Italian Journal of Mammalogy 24, 103-09.

Helmuth, H., 1968. Einige Maße des Processus Mastoideus beim Menschen und seine Bedeutung für die Geschlechtsbestimmung. Zeitschrift für Morphologie und Anthropologie 60, 75-84.

Hofmann, K., 2010. Das Hallstattzeitliche Fürstengrab vom Frankfurter Stadtwald, in: E. Wamers (Eds.), Fürsten, Feste, Rituale – Bilderwelten zwischen Kelten und Etruskern [Eine Ausstellung des Archäologischen Museums Frankfurt, 30. Oktober 2010 bis 20. März 2011]; Archäologisches Museum Frankfurt, Frankfurt am Main, pp. 65-74.

Hublin, J. J., 2002. Northwestern African Middle Pleistocene Hominids and Their Bearing on the Emergence of Homo Sapiens, in: Barham, L., Robson-Brown, K. (Eds.), Human Roots, Africa and Asia in the Middle Pleistocene. CHERUB, Western Academic and Specialist Press Lmtd, Bristol, pp. 99-121.

Krausse, D., 1996. Hochdorf III: Das Trink- und Speiseservice aus dem Späthallstattzeitlichen Fürstengrab von Eberdingen-Hochdorf (Kr. Ludwigsburg). Berichte zur Vor- und Frühgeschichte in Baden-Württemberg, Vol. 64. Konrad Theiss Verlag GmbH & Co., Stuttgart.

Martin, R., 1928. Lehrbuch der Anthropologie: In Systematischer Darstellung mit Besonderer Berücksichtigung der Anthropologischen Methoden; Für Studierende, Ärzte und Forschungsreisende, Vol 2: Kraniologie, Osteologie. G. Fischer, Jena.

Mitteroecker, P., Gunz, P., 2009. Advances in Geometric Morphometrics. Evolutionary Biology 36, 235-47.

Müller F., Jud, P., Alt, K. W., 2008. Artefacts, Skulls and Written Sources: The Social Ranking of a Celtic Family Buried at Münsingen-Rain. Antiquity 82, 462-69.

Pearson, K., 1899. Iv. Mathematical Contributions to the Theory of Evolution. - V. On the Reconstruction of the Stature of Prehistoric Races. Philosophical Transactions of the Royal Society of London. Series A, Containing Papers of a Mathematical or Physical Character 192, 169-244.

Pearson, O.M., Lieberman, D.E., 2004. The Aging of Wolff's »Law«: Ontogeny and Responses to Mechanical Loading in Cortical Bone. American Journal of Physical Anthropology: The Official Publication of the American Association of Physical Anthropologists 125, 63-99.

Pirttiniemi,P., Lahtela, P., Huggare, J., Serlo, W., 1989. Head Posture and Dentofacial Asymmetries in Surgically Treated Muscular Torticollis Patients. Acta Odontologica Scandinavica 47, 193-97.

R Development Core Team, RFFSC, 2014. R: A Language and Environment for Statistical Computing. R Foundation for Statistical Computing Vienna, Austria.

Rehbach, N. J., Willms, C., Flohr, S., Hammerl, J., Protsch von Zieten, R., 2003. Der Keltenfürst aus Frankfurt am Main – eine anthropologische und paläopathologische Analyse. Beiträge zur Archäozoologie und prähistorischen Anthropologie 4, 57-59

Rehbach, N. J., Hammerl, J., Flohr, S., Protsch von Zieten, R., 2002. Anthropologisches Gutachten zum Keltenfürsten aus Eichlehen, Hügel 1/Grab 12, in: Willms, C. (Eds.), Der Keltenfürst aus Frankfurt: Macht und Totenkult um 700 v. Chr. Frankfurts Archäologie, Vol. 21. Museum für Vor-und Frühgeschichte, Frankfurt am Main, pp. 102-107.

Rodríguez, J. I., Palacios, J., García-Alix, A., Pastor, I., Paniagua, R., 1988. Effects of Immobilization on Fetal Bone Development. A Morphometric Study in Newborns with Congenital Neuromuscular Diseases with Intrauterine Onset. Calcified Tissue International, 43, 335-39.

Ruff, C., Holt, B., Trinkaus, E., 2006. Who's Afraid of the Big Bad Wolff?: »Wolff's Law« and Bone Functional Adaptation. American Journal of Physical Anthropology: The Official Publication of the American Association of Physical Anthropologists 129, 484-98.

Schünke, M., 2000. Funktionelle Anatomie-Topographie und Funktion des Bewegungssystems. Georg Thieme Verlag, Stuttgart.

Slice, D.E., 2007. Geometric Morphometrics. Annual Review of Anthropology 36, 261-81.

Tomczak, K.K., Rosman, N. P., 2013. Torticollis. Journal of Child Neurology 28, 365-78.

Willms, C., 2002. Der Keltenfürst aus Frankfurt: Macht und Totenkult um 700 v. Chr. Frankfurts Archäologie, Vol. 19. Museum für Vor- und Frühgeschichte, Frankfurt am Main.

Willms, C., 2010. Metallzeiten. Frankfurts Archäologie, Vol. 21. Museum für Vor- und Frühgeschichte, Frankfurt am Main.

Wolff, J., 1893. Das gesetz der transformation der Knochen. Deutsche Medizinische Wochenschrift, 19, 1222-1224.

Yu, C.C., Wong, F.H., Lo, L.J., Chen, Y.R., 2004. Craniofacial Deformity in Patients with Uncorrected Congenital Muscular Torticollis: An Assessment from Three-Dimensional Computed Tomography Imaging. Plastic and Reconstructive Surgery 113, 24-33.

Zelditch, M. L., Swiderski, D.L., Sheets, H. D., 2012. Geometric Morphometrics for Biologists: A Primer. Elseviere Academic Press, New York.

Zollikofer, C.P.E., Ponce de León, M.S., Lieberman, D.E., Guy, F., Pilbeam, D., Likius, A., Mackaye, H.T., Vignaud, P., Brunet, M., 2005. Virtual Cranial Reconstruction of Sahelanthropus Tchadensis. Nature 434, 755.